European Geosciences Union

Large scale detachment folding of thermally softened crust within a closing orocline in the Chinese Altai - insights from analog modeling

Tan Shu[1,3], Prokop Závada[2,3], Ondřej Krýza[2], Yingde Jiang[1], Karel Schulmann[3]

[1]Guangzhou Institute of Geochemistry, Chinese Academy of Sciences

[2]Institute of Geophysics of the Czech Academy of Science

[3]Centre for Lithospheric Research, Czech Geological Survey

Aletai, Xinjiang, NW China

I. Research Background

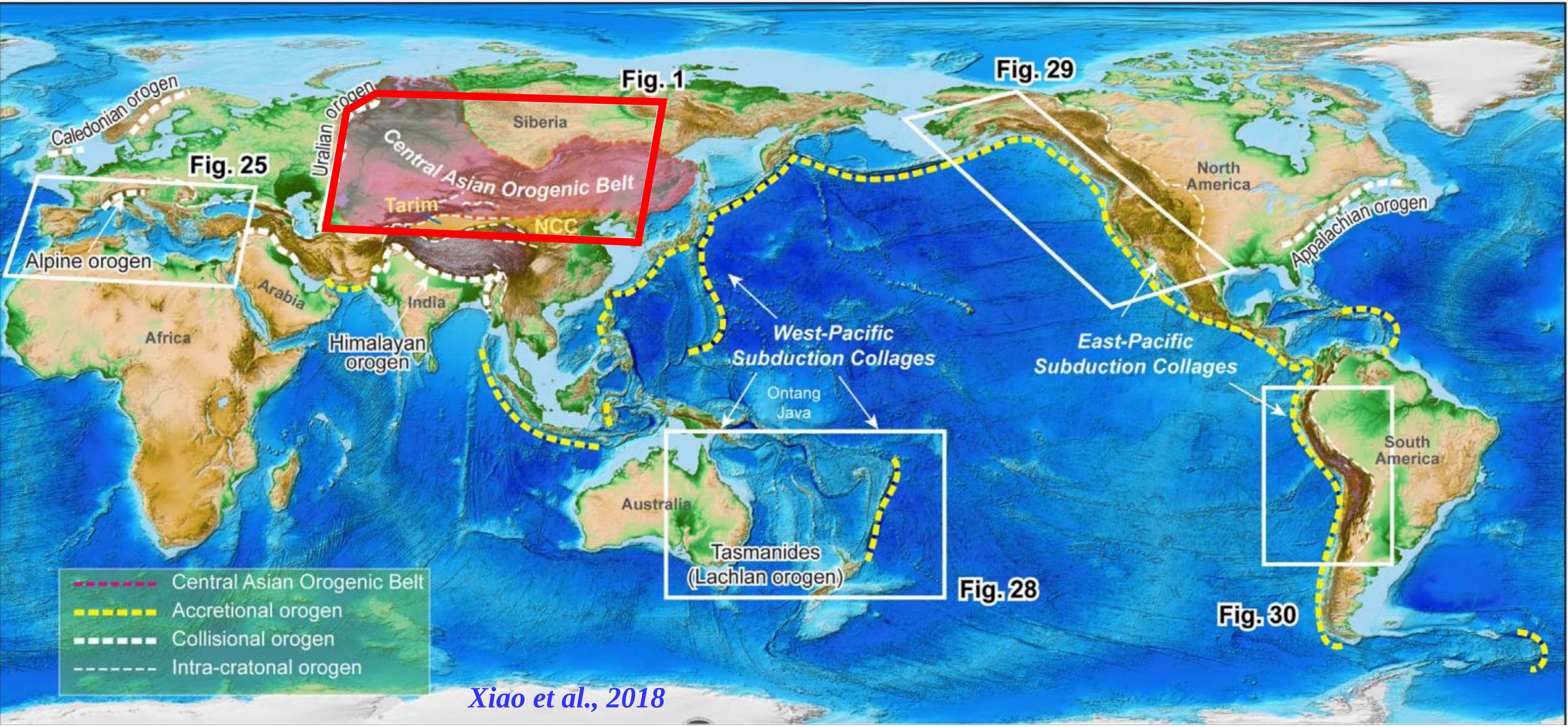

Xiao et al., 2018

CAOB: Largest accretionary orogenic belt on the earth

I. Research Background

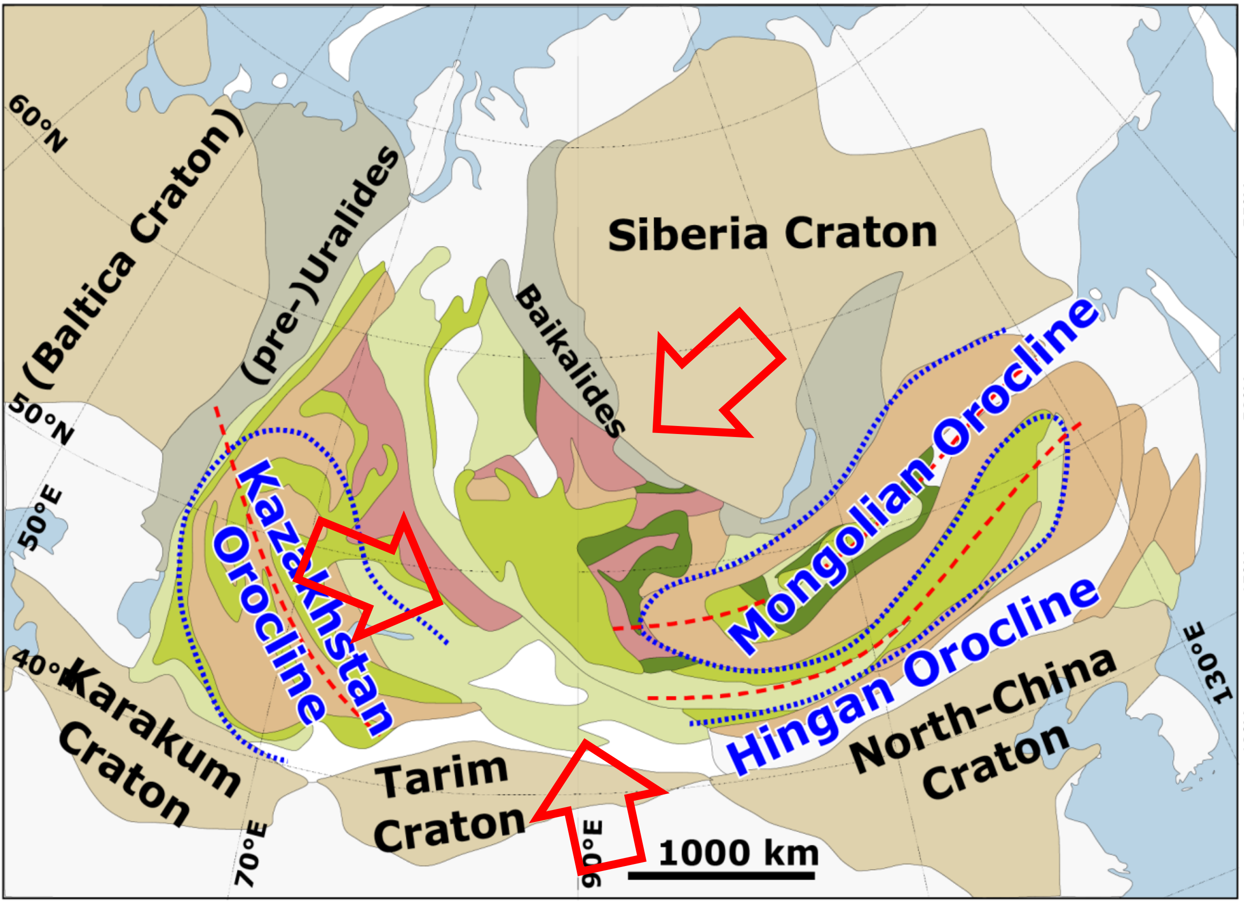

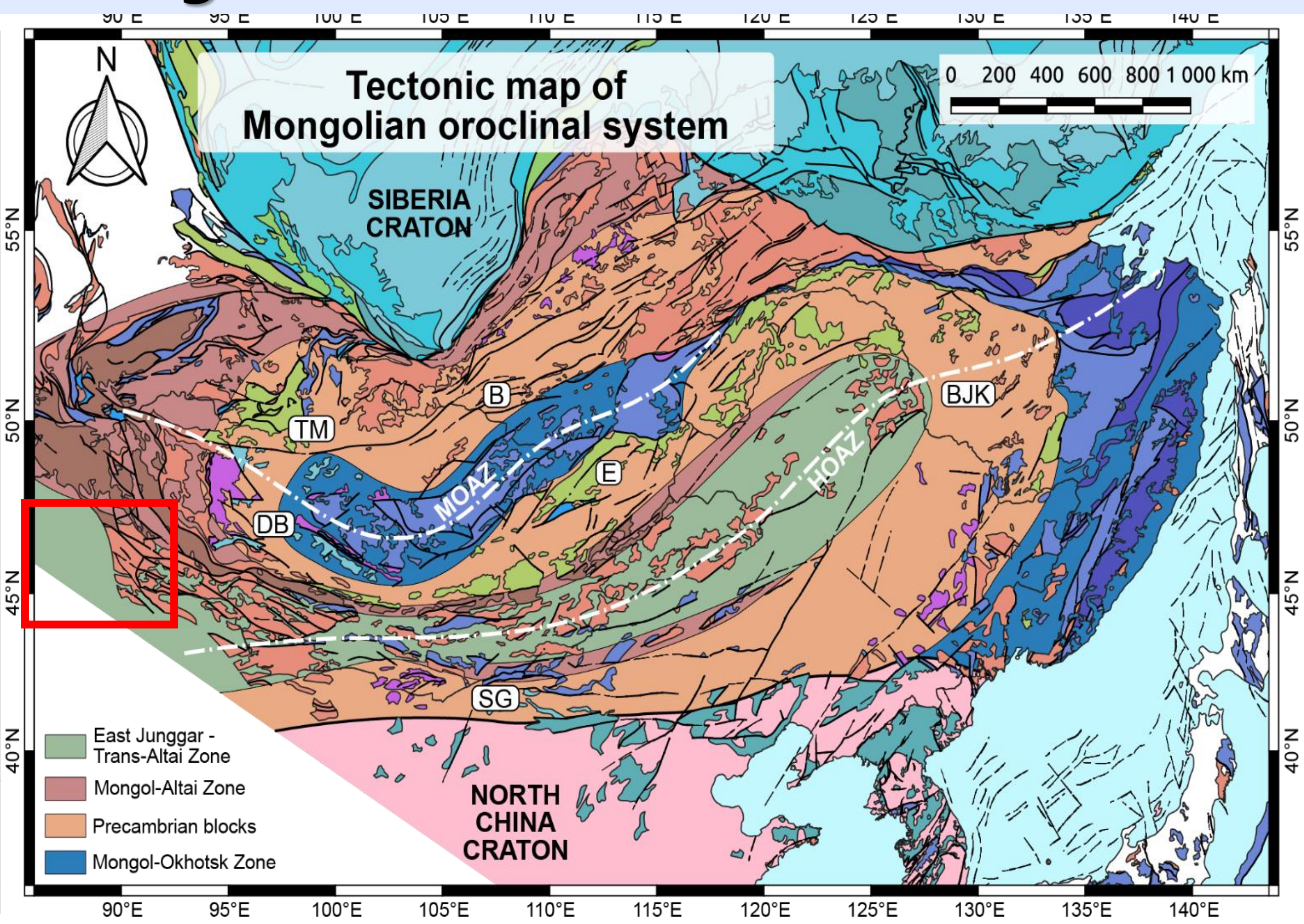

Kr ýza et al., 2019

Evolution history: from Neoproterozoic to Permian-Triassic

Complicated processes: subduction-accretion-collision (orocline bending)

Resulted in two huge Oroclines, multiple convergent orogenesis (P-T)

I. Research Background

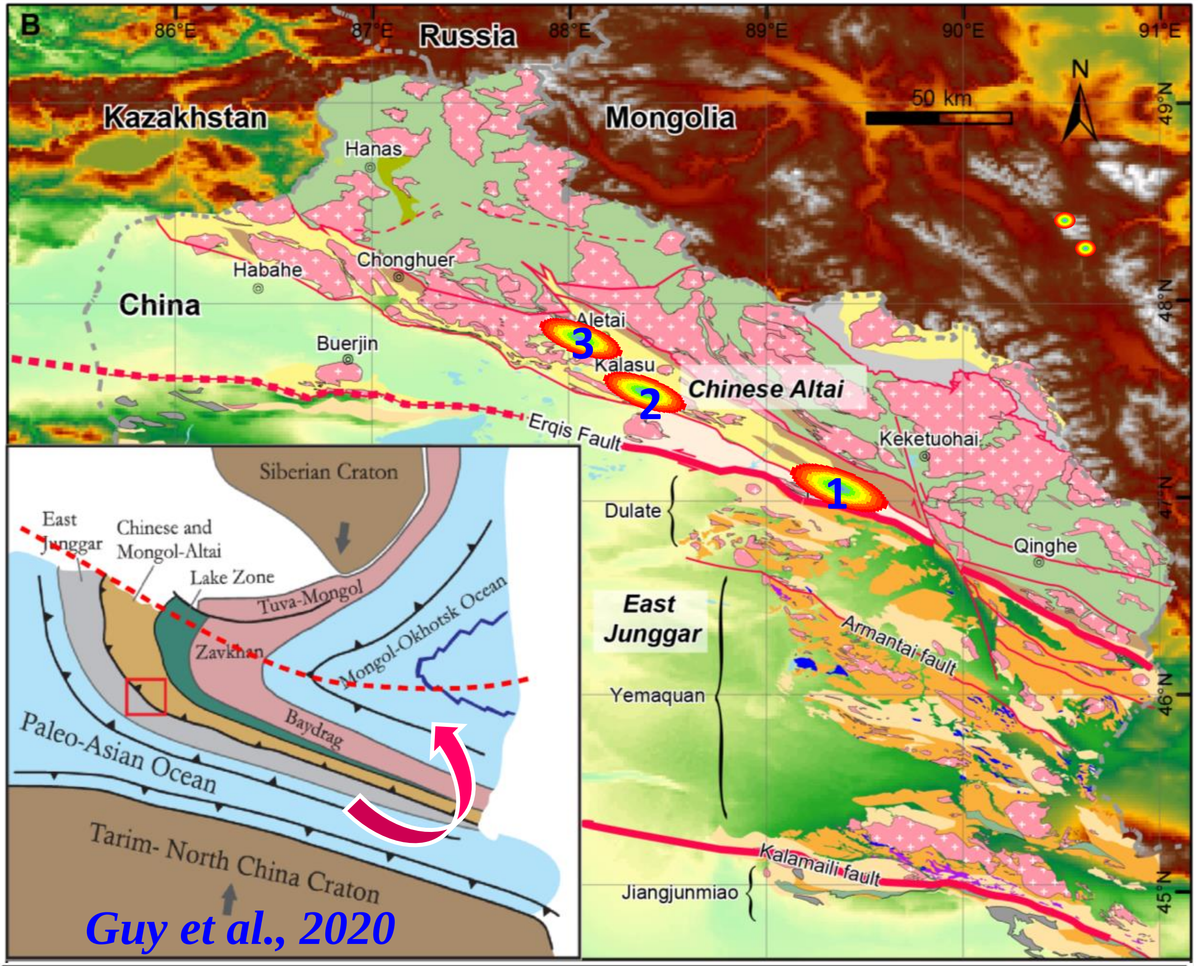

Syn-tectonic dykes ('ac-tensional fractures')

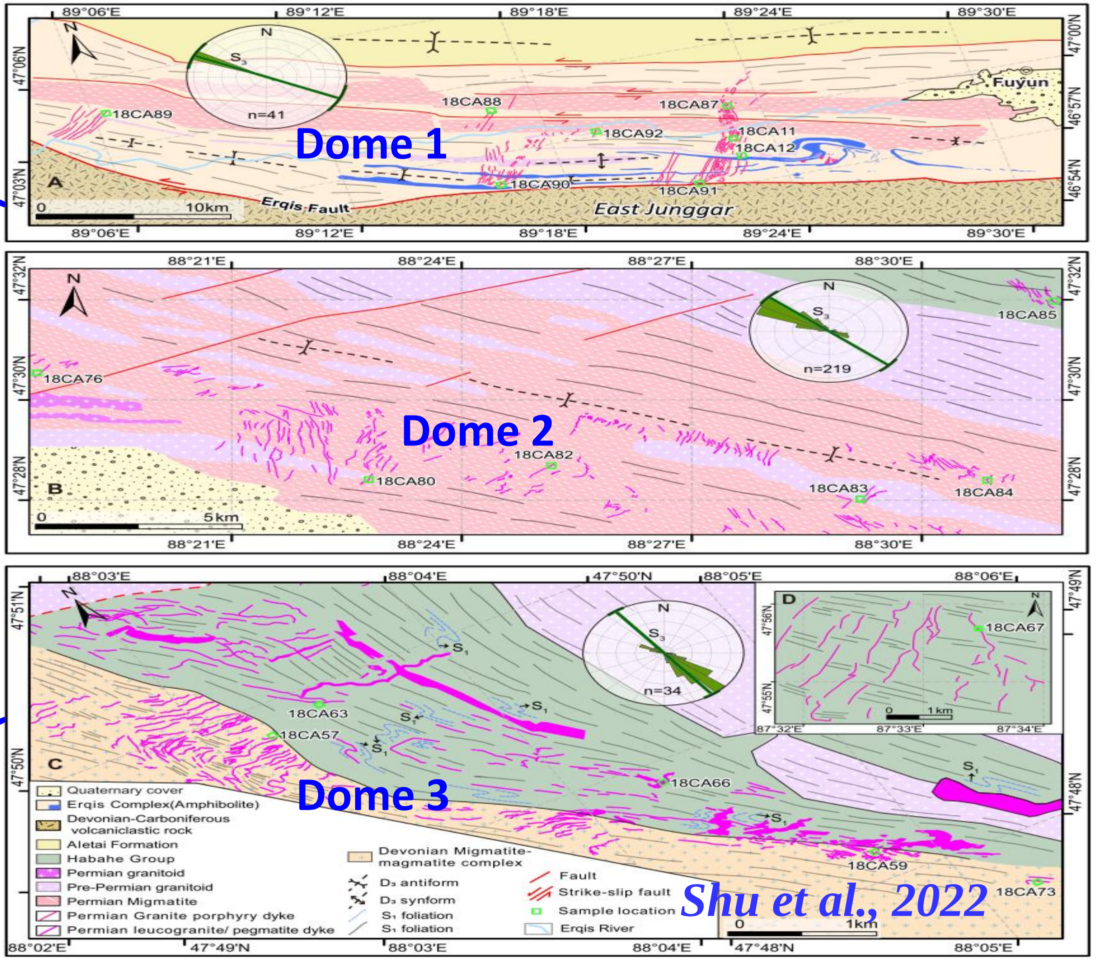

3 detachment folds in the southern Chinese Altai

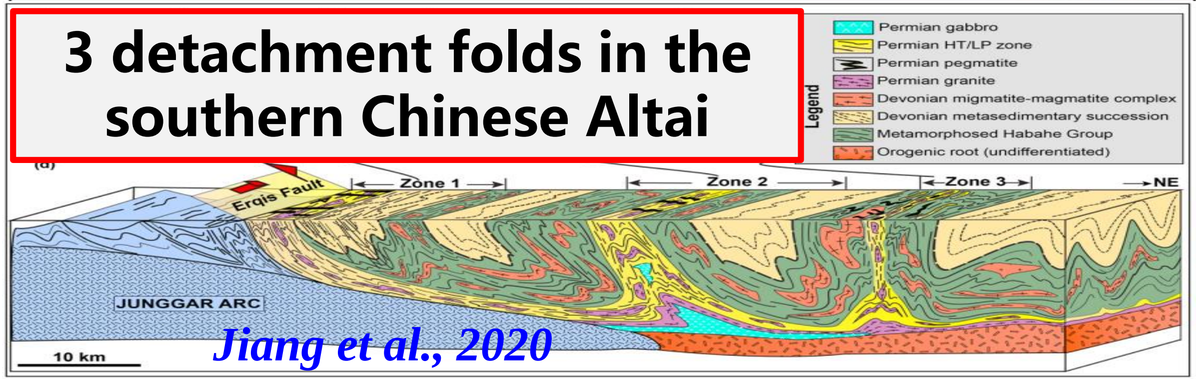

1 (south) limb of Mongolian Orocline;
2 Ribbon-like units (Chinese Altai; East Junggar);
3 detachment folds (domes) in the southern Chinese Altai, cored by migmatite-magmatite complex;
∞ syn-tectonic dykes ⊥ fold axials, S3 foliation

I. Research Background

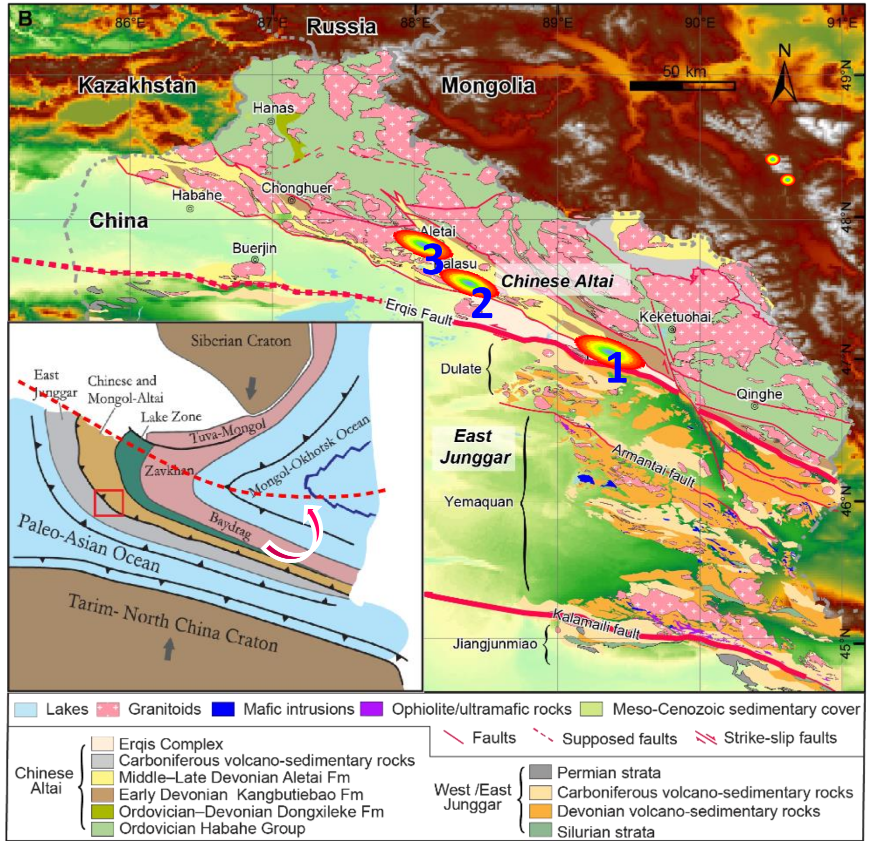

Syn-tectonic dykes
LA-ICPMS Zr/Mn U-Pb

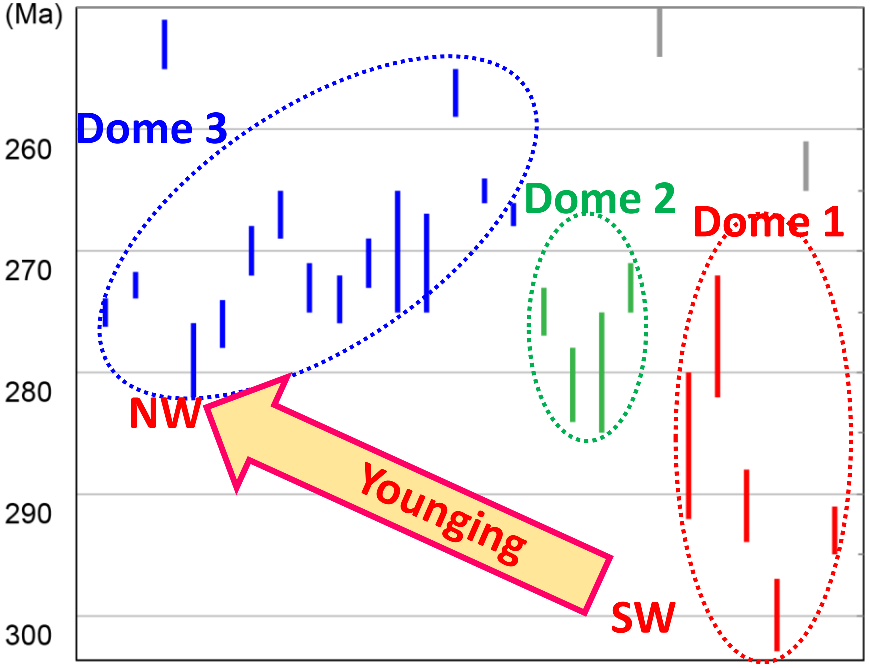

Progressive folding and propagation of fractures

High grade metamorphic rocks
Bt Ar-Ar geochronology

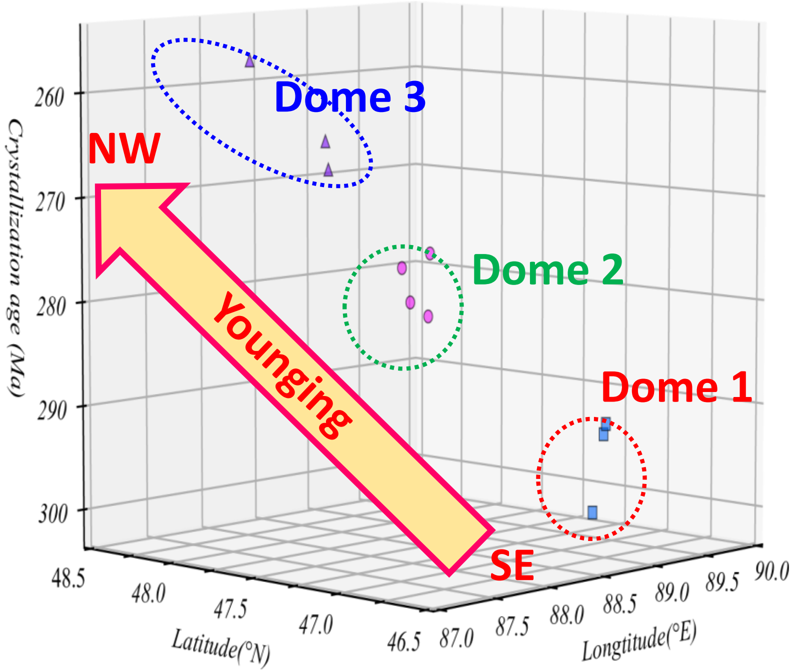

Progressive exhumation

Science questions:

How to reconstruct these detachment folds (domes) in the Chinese Altai?

How did the Mongolian Orocline affect the forming of these detachment folds?

II. Experiment Design

Apparatus (integrated with PIV method)

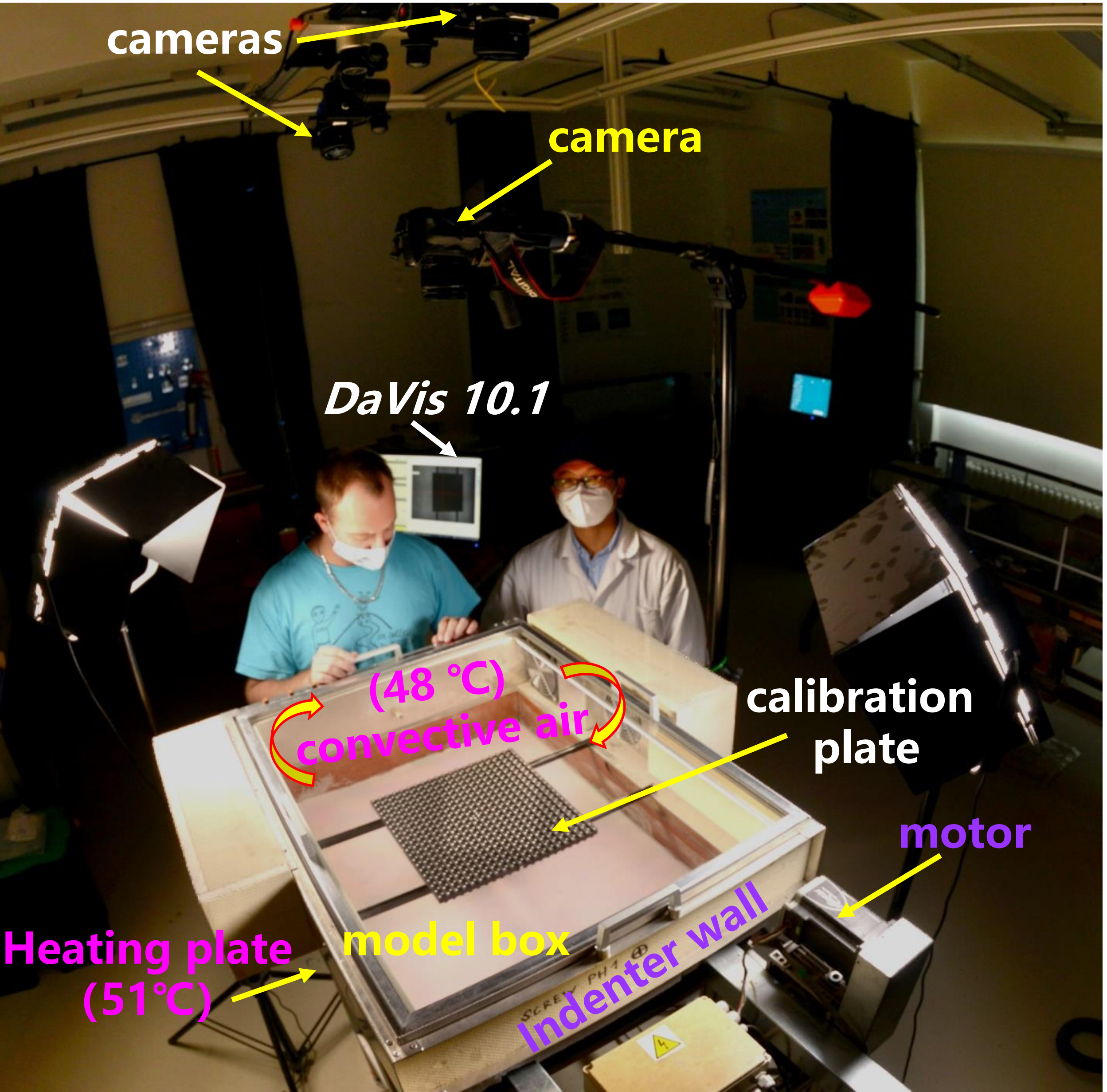

Experimental materials

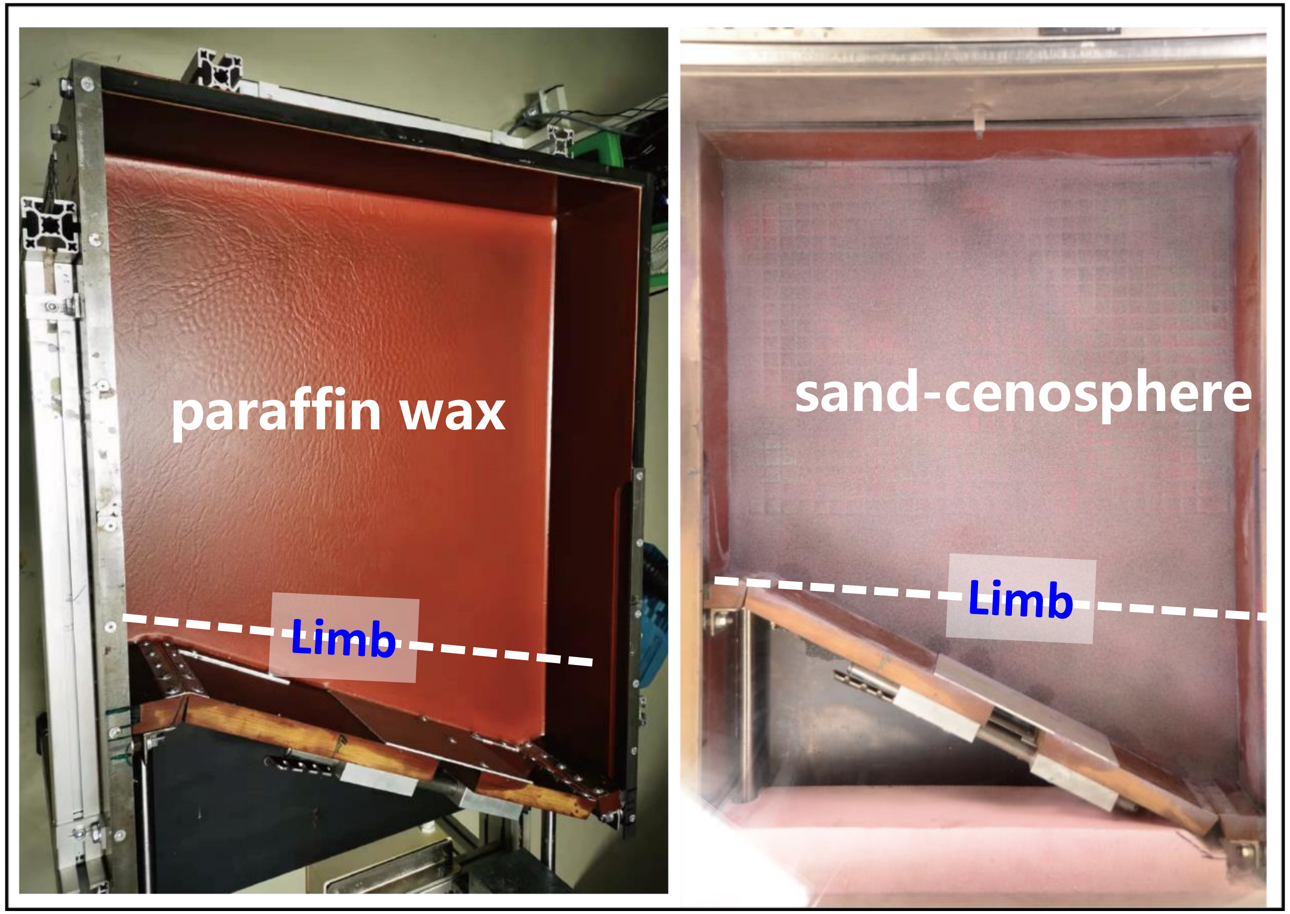

We employed analog modeling by using paraffin wax for ductile lower crust and sand-cenosphere mixture for brittle upper crust.

II. Experiment Design

Angle of convergence
α = 90°
~50% shortening

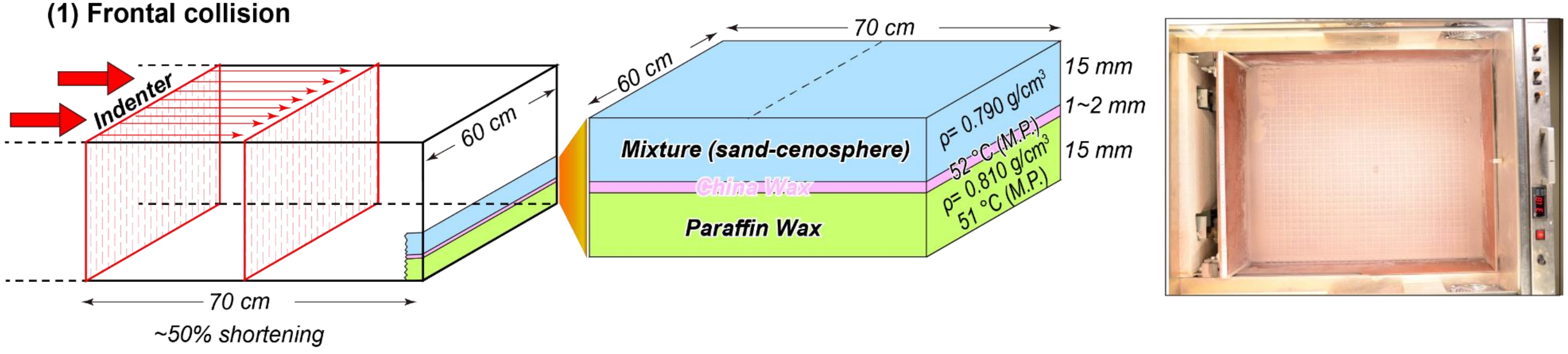

Angle of convergence
α = 65°
~50% shortening

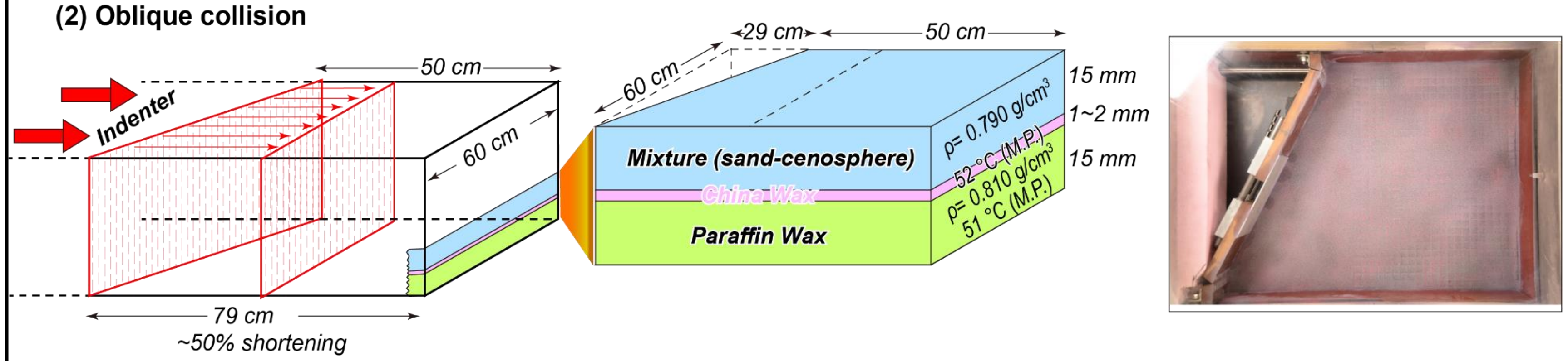

Angle of convergence
α from 60° to 90°
~47% shortening

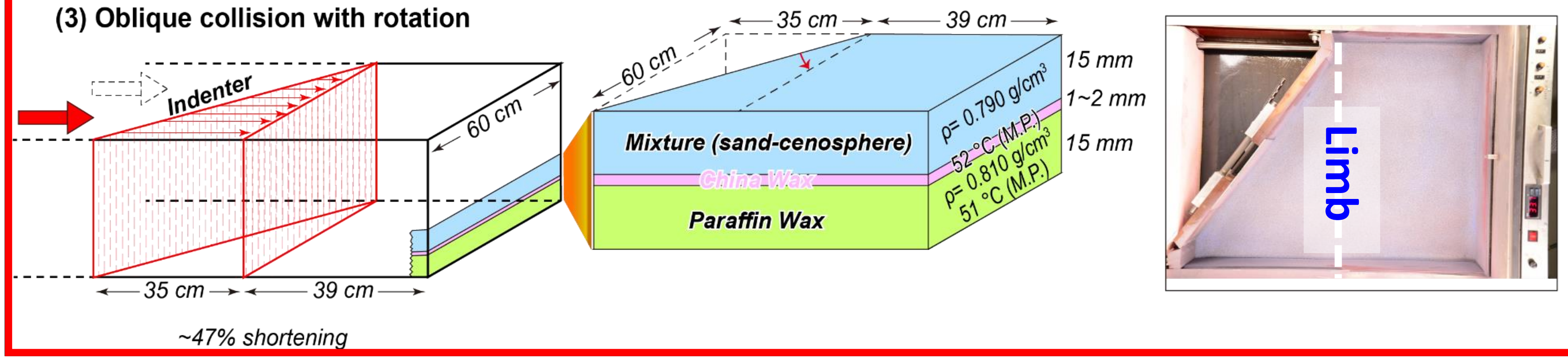

III. Results

Oblique collision with rotation

Divergence of velocity field

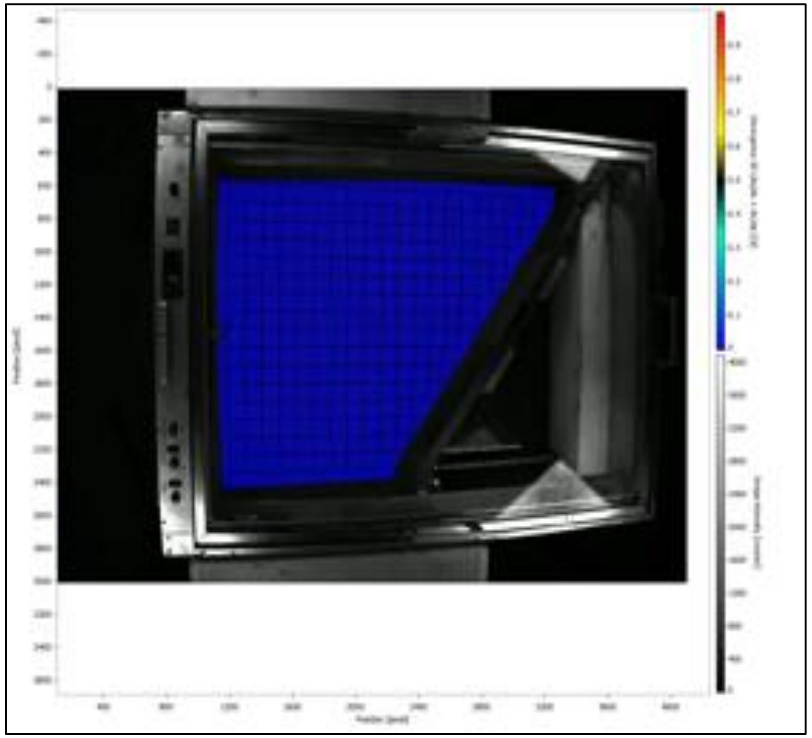

Shear strain

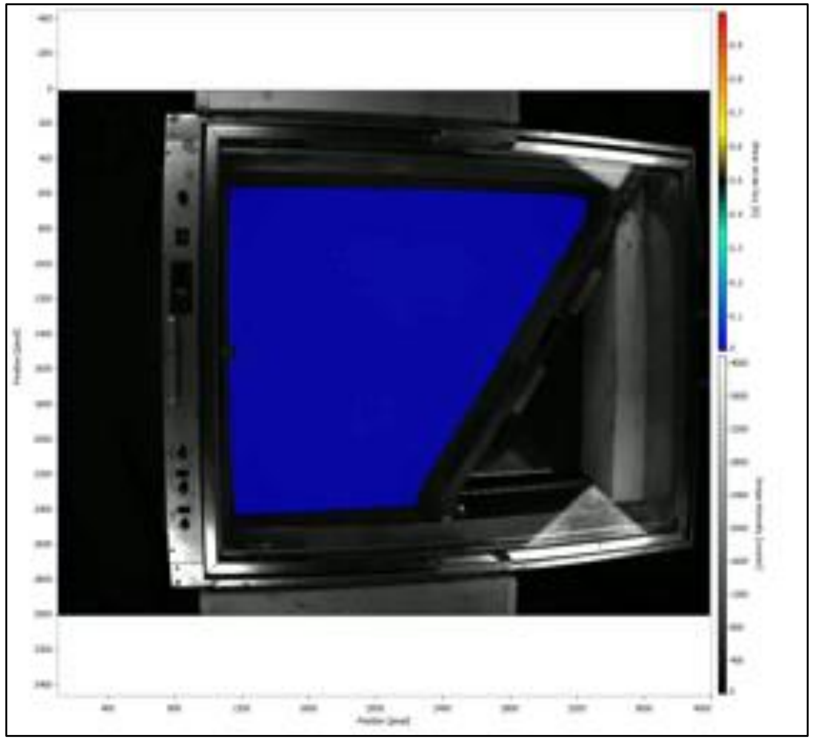

Pattern 3: Oblique Collision with rotation

Progressive development of an folds (isolated, step-like)

Divergence of velocity field： compression zone / extension zone

Shear strain: strike-slip component

III. Results

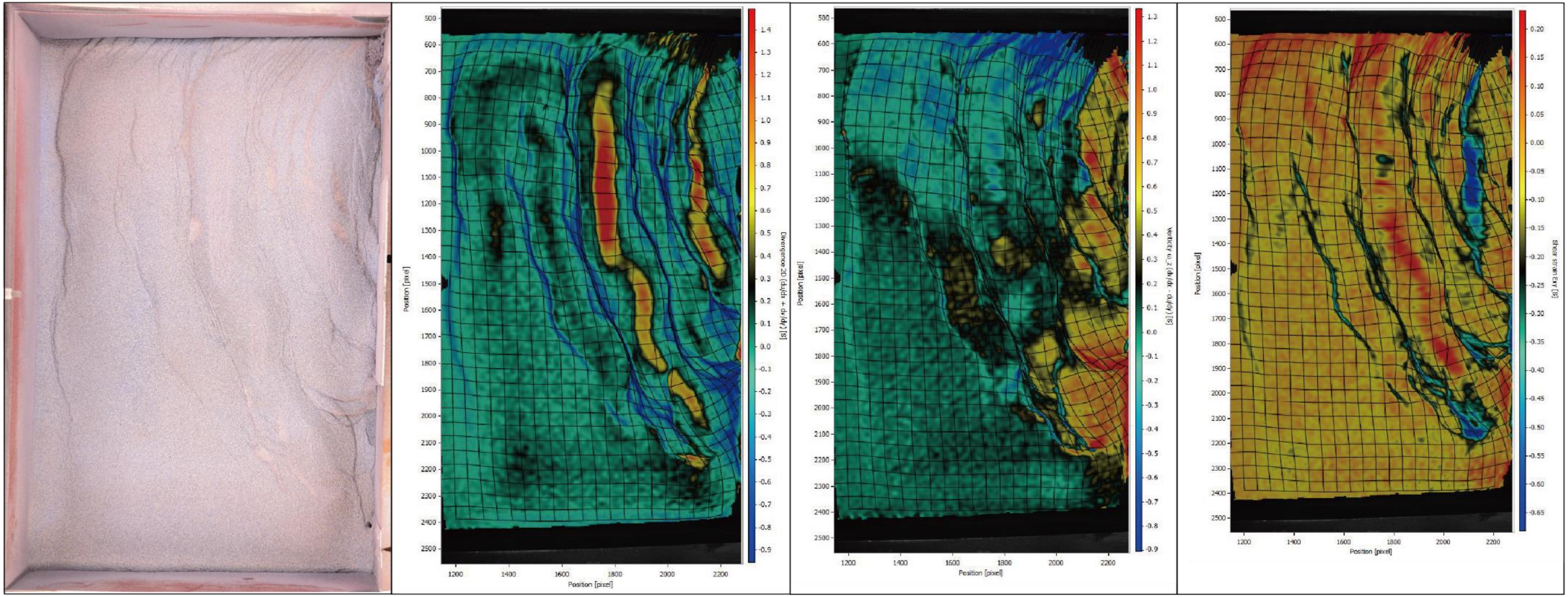

divergence of the velocity field Vorticity shear strain

Pattern 3: Oblique Collision with rotation

progressive development of an folds (isolated, step-like) with crestal-grabens that are cored by molten and partially molten wax

III. Results

Cross Sections

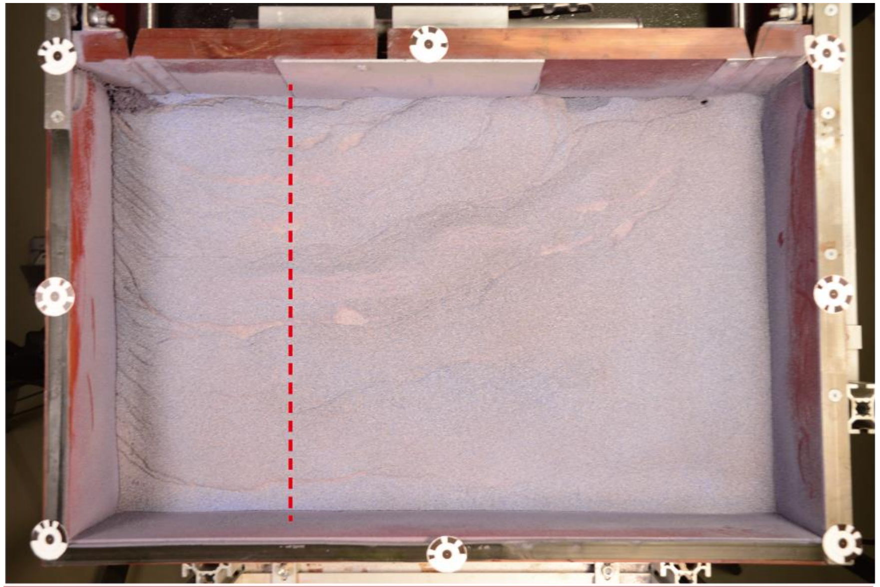

Keep the mixture

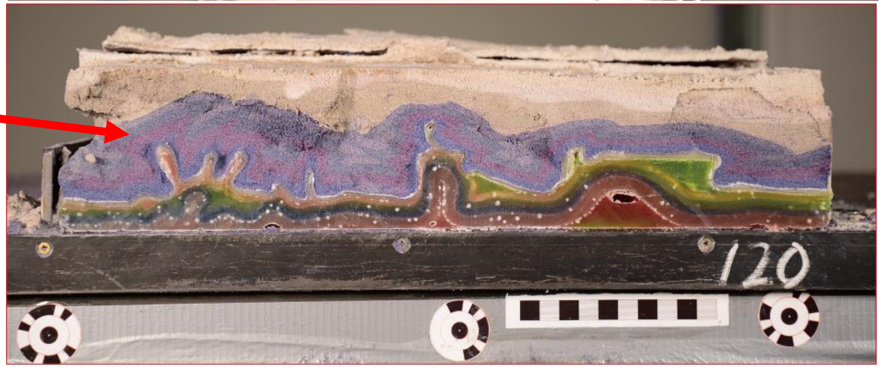

Surface

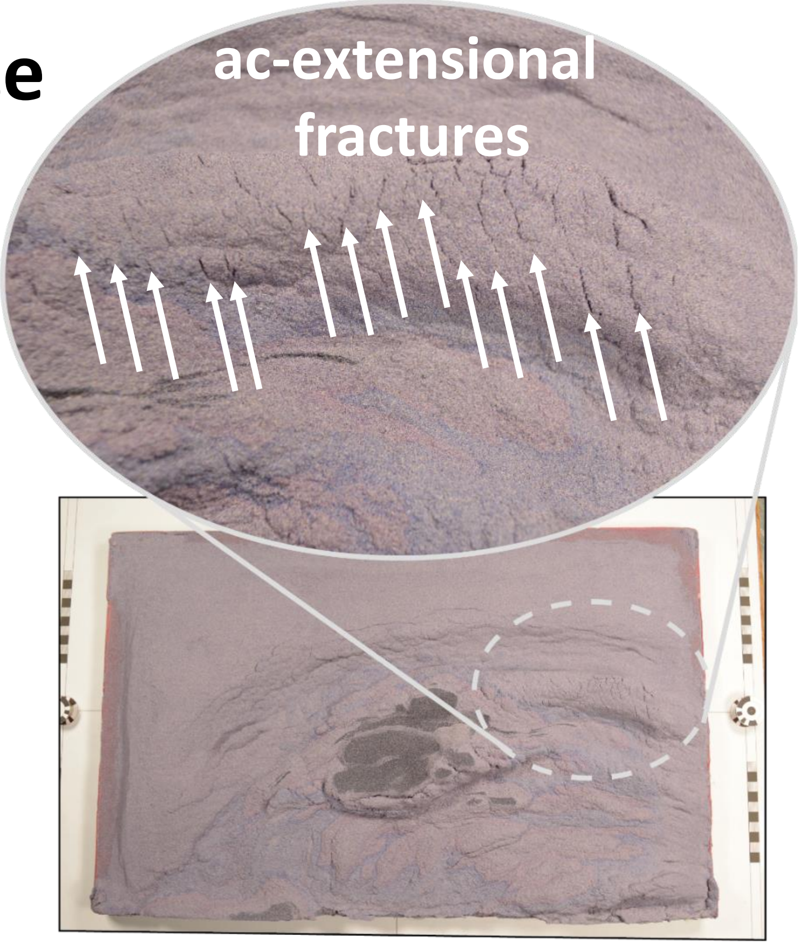

Pattern 3: Oblique Collision with rotation

The detachment folds (isolated, step-like) display with crestal-grabens that are cored by molten and partially molten wax.

Syn-tectonic dykes perpendicular to the fold axials.

III. Results

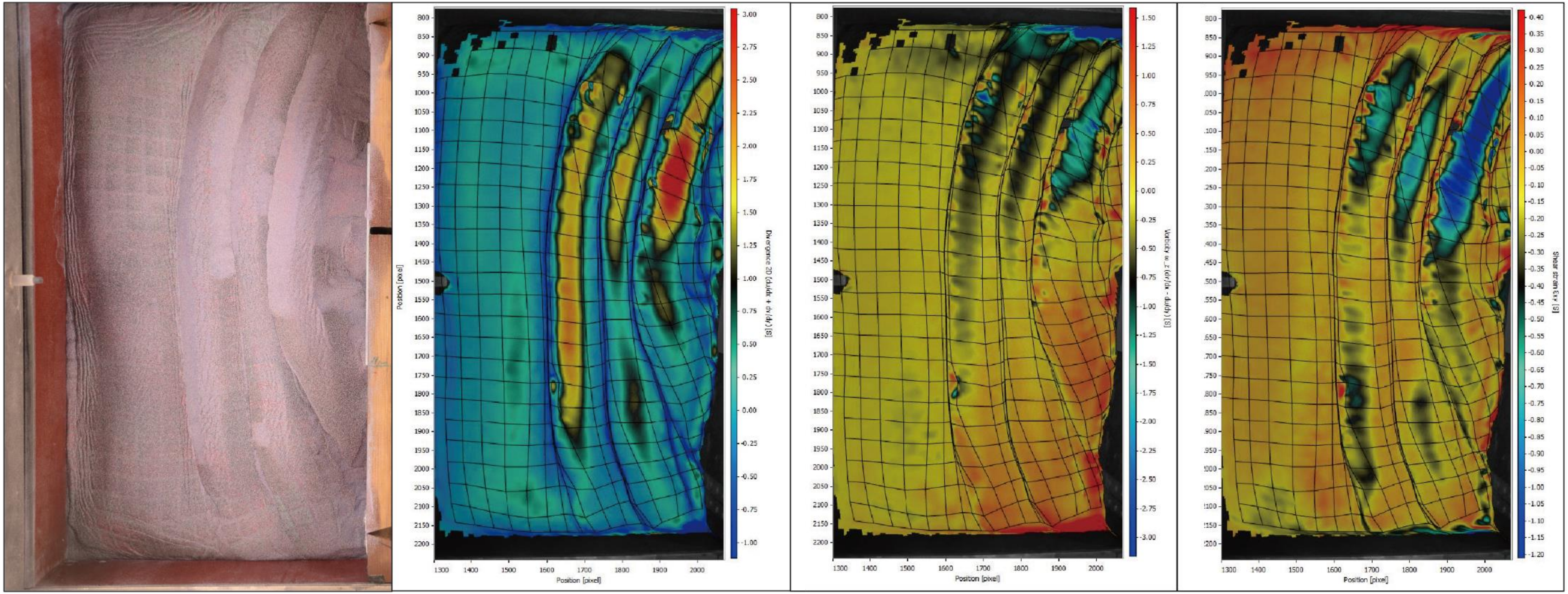

divergence of the velocity field

Vorticity

shear strain

Pattern 1-2: Frontal Collision/ Oblique Collision

Progressive development of folds with crestal-grabens that are cored by molten and partially molten wax

III. Results

Cross Sections

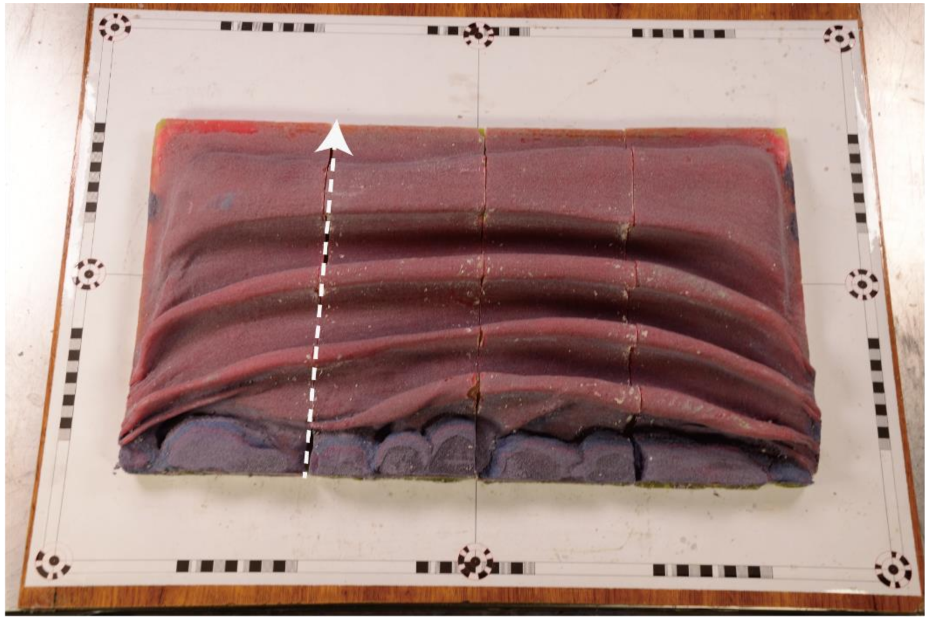

Removed the mixture

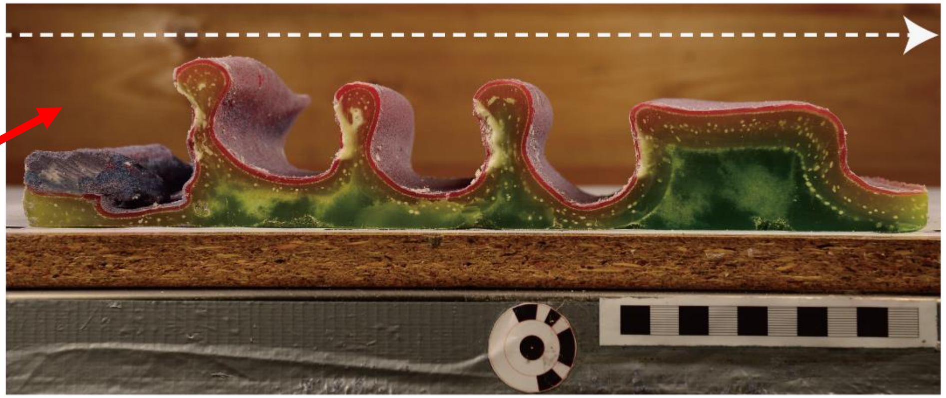

Surface

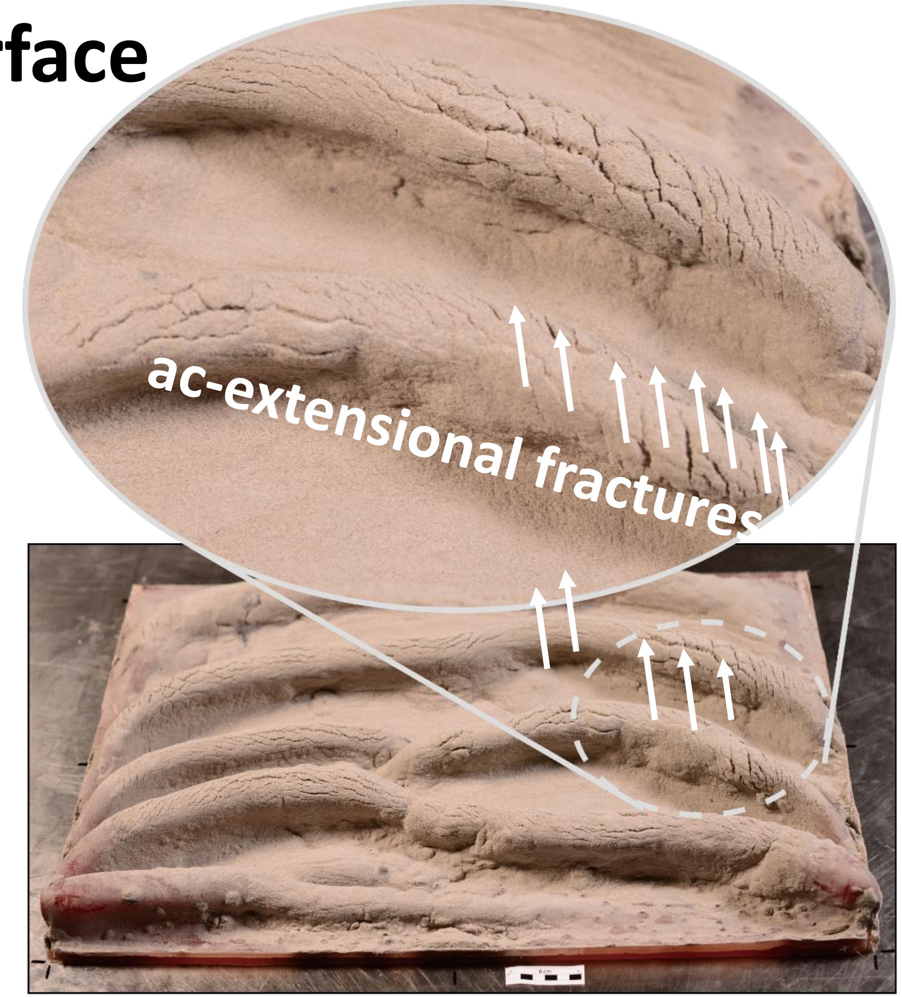

Pattern 1-2: Frontal Collision/ Oblique Collision

The detachment folds (continuous) display with crestal-grabens that are cored by molten and partially molten wax.

IV. Summary

- All models display progressive development of an array of folds with crestal-grabens that are cored by molten and partially molten wax;
- All models display considerable ac-extensional fractures that perpendicular to the fold axials;
- The frontal and oblique collision models show continuous fold traces;
- The oblique collision with rotation model shows isolated and step-like detachment folds (domes), which is consistent with the domes in southern Chinese Altai.

References

Guy, A. et al., Revision of the Chinese Altai-East Junggar terrane accretion model based on geophysical and geological constraints: Tectonics, v. 39, no. 4, p. 1-24.

Jiang, Y. D. et al., 2019, Structural and geochronological constraints on Devonian suprasubduction tectonic switching and Permian collisional dynamics in the Chinese Altai, Central Asia: Tectonics, v. 38, no. 1, p. 253-280.

Krýza, O. et al., 2020, Oroclinal buckling and associated lithospheric-scale material flow – insights from physical modelling: Implication for the Mongol-Hingan orocline: Tectonophysics.

Krýza, O. et al., 2019, Advanced strain and mass transfer analysis in crustal-scale oroclinal buckling and detachment folding analogue models: Tectonophysics, v. 764, p. 88-109.

Shu Tan et al., 2022, Structure, geochronology, and petrogenesis of Permian peraluminous granite dykes in the southern Chinese Altai as indicators of Altai–East Junggar convergence: GSA Bulletin, Accepted.

Xiao, W. J. et al., 2018, Late Paleozoic to early Triassic multiple roll-back and oroclinal bending of the Mongolia collage in Central Asia: Earth-Science Reviews, v. 186, p. 94-128.

Xiao, W. J. et al., 2015, A tale of amalgamation of three permo-triassic collage systems in central asia: Oroclines, sutures, and terminal accretion, Annual Review of Earth and Planetary Sciences, Vol 43, Volume 43, p. 477-507.

Thanks for your attention!

cugshutan@gmail.com

@frank_shu